Numer Algor
DOI 10.1007/s11075-015-0019-1

ORIGINAL PAPER

On a nonlinear mean and its application to image compression using multiresolution schemes

S. Amat[1] · J. Liandrat[2] · J. Ruiz[3] · J. C. Trillo[1]

Received: 19 October 2014 / Accepted: 15 June 2015
© Springer Science+Business Media New York 2015

Abstract This paper is devoted to the compression of colour images using a new nonlinear cell-average multiresolution scheme. The aim is to obtain similar compression properties as linear multiresolution schemes but eliminating the classical Gibbs phenomenon of this type of reconstructions near the edges. The algorithm is based on a nonlinear reconstruction operator (using a nonlinear trigonometric mean). The new reconstruction is third-order accurate in smooth regions and adapted to the presence of discontinuities. The data used are always centred with optimal support. Some theoretical properties of this scheme are analysed (order of approximation, convergence, elimination of Gibbs effect and stability).

Research supported by MICINN-FEDER MTM2010-17508 (Spain) and by 08662/PI/08 (Murcia).

✉ J. Ruiz
juan.ruiza@uah.es

S. Amat
sergio.amat@upct.es

J. Liandrat
jliandrat@ec-marseille.fr

J. C. Trillo
jc.trillo@upct.es

[1] Departamento de Matemática Aplicada y Estadística, Universidad Politécnica de Cartagena, Cartagena, Spain

[2] Ecole Superieure de Mecanique de Marseille, Laboratoire d'Analyse Topologie et Probabilites, Marseille, France

[3] Departamento de Física y Matemáticas, Universidad de Alcalá de Henares, Madrid, Spain

Published online: 03 July 2015

Keywords Cell-average multiresolution · Nonlinear subdivision scheme · Trigonometric mean · Compression · Colour images

Mathematics Subject Classifications (2010) 41A05 · 41A10 · 65D05 · 65D17

1 Introduction

In the last years, various techniques to improve the classical linear multiresolutions of wavelet type have led to nonlinear multiresolutions [1–9, 11, 13, 15, 16, 21, 22].

In this paper we are interested in a setting adapted to image applications as is the cell-average framework. In most of the considered models in the study of image processing methods, the starting point is to assume that images are L^1 functions with certain regularity. For instance, it is possible to find models working in BV, $B^1_{1,1}$ or $W^{1,1}$, [12, 14, 17]. Thus, it is natural to consider cell-average discretization operators since L^1 is the space where the original function lives.

We introduce a new nonlinear cell-average multiresolution scheme that uses a nonlinear trigonometric mean instead of the linear arithmetic mean that appears in the classical linear reconstruction (biorthogonal wavelets) or the harmonic mean of the nonlinear PPH (Piecewise Polynomial Harmonic) reconstruction [9]. The two main objectives are to eliminate the Gibbs phenomenon of linear multiresolution schemes while maintaining similar compression rates and to improve the order of PPH near critical points where the harmonic mean is zero (in this case, the PPH reduces to the first order linear scheme). We study some theoretical properties of this scheme, such as order of approximation, elimination of Gibbs effect and convergence of the associated subdivision scheme. Main attention is paid to the stability of the multiresolution scheme (crucial for practical applications).

This paper is organized as follows: In Section 2 we recall the Harten framework and we present a new nonlinear cell-average multiresolution scheme. In Section 3 we analyze some relevant theoretical properties of the scheme. Using the bivariate context of a tensor product, the new reconstruction is then tested in Section 4 on colour images, allowing to compare the performances of linear and nonlinear schemes.

2 The Harten framework

In this section we review Harten's framework for multiresolution, considering the cell-average setting.

Harten's general framework for multiresolution ([10, 19]) relies on two operators, decimation and prediction, that define the basic interscale relations. These operators act on linear vector spaces, V^k, that represent the different resolution levels (k increasing implies more resolution)

$$D_k^{k-1} : V^k \to V^{k-1} \tag{1}$$

$$P_{k-1}^{k} : V^{k-1} \to V^{k} \tag{2}$$

and they must satisfy two requirements of algebraic nature: (a) D_k^{k-1} must be a linear operator and (b) $D_k^{k-1} P_{k-1}^k = I_{V^{k-1}}$ (consistency), i.e., the identity operator on the lower resolution level represented by V^{k-1}.

In this framework, we denote by $L \in \mathbb{N}$ and 0, respectively, the finest and the coarsest resolution levels.

The Cell-average Multiresolution Setting

Let us consider a set of nested grids in $\mathbb{R}$:

$$X^k = \left\{x_j^k\right\}_{j\in\mathbb{Z}}, \quad x_j^k = jh_k, \quad h_k = 2^{-k}/N_0, \quad N_k = 2^k N_0, \quad k = 0, \ldots, L,$$

where we consider the discretization

$$\mathcal{D}_k : L^1(\mathbb{R}) \to V^k, \qquad f_j^k = (\mathcal{D}_k f)_j = \frac{1}{h_k}\int_{x_{j-1}^k}^{x_j^k} f(x)dx, \quad j \in \mathbb{Z}, \tag{3}$$

where $L^1(\mathbb{R})$ is the space of absolutely integrable functions in $\mathbb{R}$ and V^k is the space of sequences at resolution k.

In practice, the given data correspond to the finest resolution level f^L.

From the additivity of the integral, we obtain the decimation steps:

$$\begin{aligned} f_j^{k-1} &= \left(D_k^{k-1} f^k\right)_j = \frac{1}{h_{k-1}}\int_{x_{j-1}^{k-1}}^{x_j^{k-1}} f(x)dx \\ &= \frac{1}{2h_k}\int_{x_{2j-2}^k}^{x_{2j}^k} f(x)dx = \frac{1}{2}\left(f_{2j-1}^k + f_{2j}^k\right). \end{aligned}$$

The consistency requirement for P_{k-1}^k becomes

$$f_j^{k-1} = \left(D_k^{k-1} P_{k-1}^k f^{k-1}\right)_j = \frac{1}{2}\left(\left(P_{k-1}^k f^{k-1}\right)_{2j-1} + \left(P_{k-1}^k f^{k-1}\right)_{2j}\right).$$

Hence, if $f^{k-1} = D_k^{k-1} f^k$, then the two last equations imply that the prediction errors satisfy

$$e_{2j-1}^k = f_{2j-1}^k - \left(P_{k-1}^k f^{k-1}\right)_{2j-1} = \left(P_{k-1}^k f^{k-1}\right)_{2j} - f_{2j}^k = -e_{2j}^k,$$

which shows the redundancy inherent in the prediction error.

By considering only the prediction errors at (for example) the odd points of the grid X^k, we immediately obtain a one-to-one correspondence:

$$\begin{aligned} f_j^{k-1} &= \frac{f_{2j}^k + f_{2j-1}^k}{2}, \quad d_j^k = f_{2j-1}^k - \left(P_{k-1}^k f^{k-1}\right)_{2j-1}, \\ f_{2j-1}^k &= \left(P_{k-1}^k f^{k-1}\right)_{2j-1} + d_j^k, \quad f_{2j}^k = 2f_j^{k-1} - f_{2j-1}^k. \end{aligned} \tag{4}$$

Starting from the linear scheme associated to three cells

$$f_{2j-1}^k = f_j^{k-1} - \frac{1}{4}\frac{\delta f_j^{k-1} + \delta f_{j+1}^{k-1}}{2} + d_j^k, \tag{5}$$

$$f_{2j}^k = f_j^{k-1} + \frac{1}{4}\frac{\delta f_j^{k-1} + \delta f_{j+1}^{k-1}}{2} - d_j^k, \tag{6}$$

where δ is the first order difference $\left(\delta f_j^{k-1} := f_j^{k-1} - f_{j-1}^{k-1}\right)$,

In [9], the authors substitute the arithmetic mean in (5) and (6) by a nonlinear mean, obtaining the following family of prediction operators,

$$\left(P_{k-1}^k f^{k-1}\right)_{2j-1} = f_j^{k-1} - \frac{1}{4} H_2\left(\delta f_j^{k-1}, \delta f_{j+1}^{k-1}\right), \tag{7}$$

where δ is the first order difference operator defined before. Then $H_2(x, y)$ is replaced by the nonlinear harmonic mean defined in [6] as:

$$H_2(x, y) = \frac{\text{sign}(x) + \text{sign}(y)}{2}\left|\frac{2xy}{x+y}\right|. \tag{8}$$

The resulting multiresolution scheme is called PPH (Piecewise Polinomial Harmonic) and it is given by

$$f_{2j-1}^k = f_j^{k-1} - \frac{1}{4} H_2\left(\delta f_j^{k-1}, \delta f_{j+1}^{k-1}\right) + d_j^k,$$

$$f_{2j}^k = f_j^{k-1} + \frac{1}{4} H_2\left(\delta f_j^{k-1}, \delta f_{j+1}^{k-1}\right) - d_j^k,$$

As it is defined in [6] and in (8), this mean presents the disadvantage of losing order when δf_j^{k-1} and δf_{j+1}^{k-1} have different signs. In particular, it reduces to the first order linear scheme of one cell. With the aim of solving this problem, we propose the following nonlinear cell-average prediction,

$$\left(P_{k-1}^k f^{k-1}\right)_{2j-1} = f_j^{k-1} - \frac{1}{4} AT\left(\frac{\delta f_j^{k-1}}{h_{k-1}}, \frac{\delta f_{j+1}^{k-1}}{h_{k-1}}\right) h_{k-1}, \tag{9}$$

where $AT(x, y)$ is the nonlinear trigonometric mean defined as:

$$AT(x, y) = \tan\left(\frac{\arctan(x) + \arctan(y)}{2}\right). \tag{10}$$

And the new scheme writes

$$f_{2j-1}^k = f_j^{k-1} - \frac{1}{4} AT\left(\frac{\delta f_j^{k-1}}{h_{k-1}}, \frac{\delta f_{j+1}^{k-1}}{h_{k-1}}\right) h_{k-1} + d_j^k,$$

$$f_{2j}^k = f_j^{k-1} + \frac{1}{4} AT\left(\frac{\delta f_j^{k-1}}{h_{k-1}}, \frac{\delta f_{j+1}^{k-1}}{h_{k-1}}\right) h_{k-1} - d_j^k, \tag{11}$$

The three schemes presented satisfy the consistency condition.

3 Theoretical properties of the new scheme for piecewise functions

In this section we present some properties related to the new scheme. First, we denote by S_{AT} the associated subdivision scheme, that is, $f^k = S_{AT}(f^{k-1})$ (the prediction operator without considering the details):

$$f^k_{2j-1} = f^{k-1}_j - \frac{1}{4} AT\left(\frac{\delta f^{k-1}_j}{h_{k-1}}, \frac{\delta f^{k-1}_{j+1}}{h_{k-1}}\right) h_{k-1},$$
$$f^k_{2j} = f^{k-1}_j + \frac{1}{4} AT\left(\frac{\delta f^{k-1}_j}{h_{k-1}}, \frac{\delta f^{k-1}_{j+1}}{h_{k-1}}\right) h_{k-1}.$$

In this type of applications, like zoom or curve generation, the given data is f^0 and the subdivision scheme increases the resolution at each step:

$$f^0 \to f^1 \to f^2 \to \cdots$$

We will use the discrete l_1 and the l_∞ norms

$$||f^k||_1 = h_k \sum_{j\in\mathbb{Z}} |f^k_j|$$
$$||f^k||_\infty = \max_{j\in\mathbb{Z}}\{|f^k_j|\}.$$

3.1 Properties of the trigonometric mean

We start with some general properties of the introduced trigonometric mean that follow from basic calculus.

Lemma 1 *Basic properties of the trigonometric mean*

1. *If* $\min\{|x|, |y|\} = O(1)$ *then* $|AT(x, y)h| = O(h)$.
2. *If* $x = O(1)$ *and* $y = O(1)$ *then* $|\frac{x+y}{2} - AT(x, y)| = O((x - y)^2)$.

The first property is related to the adaption to singularities (Gibbs phenomenon) and the second to the order of approximation.

3.2 Order of approximation

We recall the following definition.

Definition 1 Order of approximation:
A dyadic subdivision scheme S is said to have an order s of approximation if for any function $g \in C^s$ and all $h > 0$, if $f^0 = \{g(jh)\}_{j\in\mathbb{Z}}$ then

$$|Sf^0_j - g(2^{-1}jh)| \le Ch^s.$$

Concerning the order of approximation the following result holds.

Proposition 1 *Order of approximation:*
For any function $g \in C^3(\mathbb{R})$ *and* $h > 0$, *if* $f^0 = \{g(jh)\}_{j\in\mathbb{Z}}$, *then*

$$|(S_{AT} f)_j - g(2^{-1} jh)| = O(h^3).$$

Proof For all $j \in \mathbb{Z}$,

$$\left| AT\left(\frac{\delta f_j^k}{h_k}, \frac{\delta f_{j+1}^k}{h_k}\right) h_k - \frac{\frac{\delta f_j^k}{h_k} + \frac{\delta f_{j+1}^k}{h_k}}{2} h_k \right| = O\left(h_k^3\right).$$

Since the original linear scheme is of order of approximation 3 we get the result. □

3.2.1 New scheme versus PPH scheme

In this subsection we perform a one dimensional test in order to identify the advantages of using the trigonometric mean instead of the harmonic mean. As mentioned before, the PPH method reduces its accuracy to the first order linear method when the arguments of the harmonic mean have different signs. This is due to the fact that it can appear a zero division in the case mentioned. On the other hand, the nonlinear trigonometric mean proposed in this article, overcomes this problem. We have no more than looking at expressions (8) and (10) to realise this fact. As it can be observed in expression (10), the case when the arguments of the mean have different signs would not affect the order of the expression shown in (10). Figure 1 shows the error of both algorithms when compressing a signal with a very high tolerance, (i.e. no details are kept). The grid has been set from -10.076 to 10 in order to assure that the change of sign of the derivative of the function never coincides with the position of zero in the discretization of the function. Table 1 shows the results obtained when compressing vectors of different lengths of the function $y = x^2$ defined in the previous interval $(-10.076, 10)$ and using also a very high tolerance. We can see that for the new method the l_∞ norm and the l_1 norm belong to the same order of magnitude. This means that the error belongs to the same order of magnitude for the whole signal. For the PPH, as there are places where the method has lost order, there will be places where the error of approximation is greater. Thus, the l_∞ norm will be greater than the l_1 norm. This is what we can see in Table 1.

3.3 Elimination of the Gibbs phenomenon

According to D. Gottlieb and C.W. Shu [18], given a punctually discontinuous function g and its sampling f^0 defined by $f^0 = \{g(jh)\}_{j\in\mathbb{Z}}$, the Gibbs phenomenon deals with the convergence of $S^\infty(f^0)$ towards g when h goes to 0. It can be characterized by two features ([18]):

1. Away from the discontinuity the convergence is rather slow and for any point x,

$$|g(x) - S^\infty(f^0)(x)| = O(h).$$

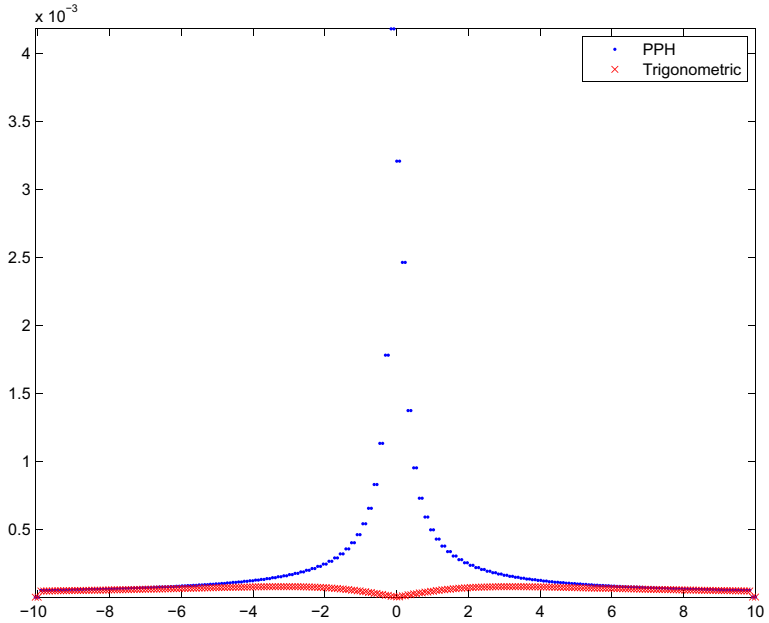

Fig. 1 Error obtained by the PPH and the new algorithm when compressing the function $y = x^2$ with a high tolerance

2. There is an overshoot, close to the discontinuity, that does not diminish when reducing h. Thus,

$$\max |g(x) - S^{\infty}(f^0)(x)| \text{ does not tend to zero with } h.$$

We are now going to prove that the nonlinear scheme S_{AT} does not suffer from the Gibbs phenomenon oscillations.

Table 1 Norm l_1 and l_∞, and rate of convergence of the error obtained when compressing vectors of different lengths (256, 512 and 1024) of the function $y = x^2$ defined in the interval $(-10.076, 10)$ using a high tolerance

	New Method			PPH		
Length	256	512	1024	256	512	1024
l_1	5.7e-5	3.74e-6	1.8e-7	2.5e-4	3.28e-5	5.5e-6
Order	–	3.9299	4.3770	–	2.9302	2.5762
l_∞	7.6e-5	4.76e-6	2.8e-7	4.1e-3	7.8e-4	3.6e-4
Order	–	3.9970	4.0875	–	2.3941	1.1155

By definition, the scheme is given by

$$f_{2j-1}^{k} = f_{j}^{k-1} - \frac{1}{4} AT\left(\frac{\delta f_{j}^{k-1}}{h_{k-1}}, \frac{\delta f_{j+1}^{k-1}}{h_{k-1}}\right) h_{k-1},$$

$$f_{2j}^{k} = f_{j}^{k-1} + \frac{1}{4} AT\left(\frac{\delta f_{j}^{k-1}}{h_{k-1}}, \frac{\delta f_{j+1}^{k-1}}{h_{k-1}}\right) h_{k-1}.$$

Without loss of generality, lets take a particular set of data $\{\cdots, f_0^0\, f_1^0, f_2^0, f_3^0, \cdots\}$. Lets suppose that the data is piecewise smooth and that there is a jump discontinuity placed at the cell $[x_1^0, x_2^0]$, that corresponds to the value f_2^0. Now, if we try to go from the scale f^0 to the scale f^1, we can obtain $\{\cdots, f_1^1, f_2^1, f_3^1, f_4^1, \cdots\}$ Mind that the values before f_1^1 and after f_4^1 are not affected by the discontinuity, thus the method only uses information from regularity zones,

$$\cdots$$

$$f_1^1 = f_1^0 - \frac{1}{4} AT\left(\frac{\delta f_1^0}{h_0}, \frac{\delta f_2^0}{h_0}\right) h_0,$$

$$f_2^1 = f_1^0 + \frac{1}{4} AT\left(\frac{\delta f_1^0}{h_0}, \frac{\delta f_2^0}{h_0}\right) h_0,$$

$$f_3^1 = f_2^0 - \frac{1}{4} AT\left(\frac{\delta f_2^0}{h_0}, \frac{\delta f_3^0}{h_0}\right) h_0,$$

$$f_4^1 = f_2^0 + \frac{1}{4} AT\left(\frac{\delta f_2^0}{h_0}, \frac{\delta f_3^0}{h_0}\right) h_0,$$

$$\cdots$$

It is important to note that, due to property 1 of Lemma 1, $AT \equiv O(h_0)$ in the four previous cases. Thus, there is no Gibbs phenomenon.

Now we can go from the scale f^1 to the scale f^2

$$\cdots$$

$$f_1^2 = f_1^1 - \frac{1}{4} AT\left(\frac{\delta f_1^1}{h_1}, \frac{\delta f_2^1}{h_1}\right) h_1,$$

$$f_2^2 = f_1^1 + \frac{1}{4} AT\left(\frac{\delta f_1^1}{h_1}, \frac{\delta f_2^1}{h_1}\right) h_1,$$

$$f_3^2 = f_2^1 - \frac{1}{4} AT\left(\frac{\delta f_2^1}{h_1}, \frac{\delta f_3^1}{h_1}\right) h_1,$$

$$f_4^2 = f_2^1 + \frac{1}{4} AT\left(\frac{\delta f_2^1}{h_1}, \frac{\delta f_3^1}{h_1}\right) h_1,$$

$$
\begin{aligned}
f_5^2 &= f_3^1 - \frac{1}{4} AT\left(\frac{\delta f_1^3}{h_1}, \frac{\delta f_4^1}{h_1}\right) h_1, \\
f_6^2 &= f_3^1 + \frac{1}{4} AT\left(\frac{\delta f_1^3}{h_1}, \frac{\delta f_4^1}{h_1}\right) h_1, \\
f_7^2 &= f_4^1 - \frac{1}{4} AT\left(\frac{\delta f_4^1}{h_1}, \frac{\delta f_4^1}{h_1}\right) h_1, \\
f_8^2 &= f_4^1 + \frac{1}{4} AT\left(\frac{\delta f_4^1}{h_1}, \frac{\delta f_5^1}{h_1}\right) h_1, \\
&\cdots
\end{aligned}
$$

From the first step, we obtain

$$
\begin{aligned}
&\cdots \\
f_1^2 &= f_1^0 - \frac{1}{4} AT\left(\frac{\delta f_1^0}{h_0}, \frac{\delta f_2^0}{h_0}\right) h_0 - \frac{1}{4} AT\left(\frac{\delta f_1^1}{h_1}, \frac{\delta f_2^1}{h_1}\right) h_1, \\
&\cdots \\
f_5^2 &= f_2^0 - \frac{1}{4} AT\left(\frac{\delta f_2^0}{h_0}, \frac{\delta f_3^0}{h_0}\right) h_0 - \frac{1}{4} AT\left(\frac{\delta f_3^1}{h_1}, \frac{\delta f_4^1}{h_1}\right) h_1, \\
&\cdots
\end{aligned}
$$

by definition

$$
\begin{aligned}
&\cdots \\
\delta f_1^1 &= f_1^1 - f_0^1 = (f_1^0 - f_0^0) - \frac{1}{4} AT\left(\frac{\delta f_1^0}{h_0}, \frac{\delta f_2^0}{h_0}\right) h_0 - \frac{1}{4} AT\left(\frac{\delta f_0^0}{h_0}, \frac{\delta f_1^0}{h_0}\right) h_0 \\
&\cdots
\end{aligned}
$$

It is important to note that at regularity zones, $\frac{\delta f^k}{h_k} \approx f'$ and that the absolute value of the derivative $|f'|$ is bounded. Thus, at those zones, there exists M such that

$$\left|\frac{\delta f^k}{h_k}\right| \leq M.$$

Using the first property of the mean in Lemma 1, we can conclude that for any scale k we have,

$$
\begin{aligned}
&\cdots \\
|f_\cdot^k - f_1^0| &\leq \frac{h_0 M}{4} \sum_{l=1}^{\infty} \frac{1}{2^l} \leq \frac{h_0 M}{4} \frac{1}{1-\frac{1}{2}} = \frac{h_0 M}{2}, \\
&\cdots \\
|f_\cdot^k - f_2^0| &\leq \frac{h_0 M}{4} \sum_{l=1}^{\infty} \frac{1}{2^l} \leq \frac{h_0 M}{4} \frac{1}{1-\frac{1}{2}} = \frac{h_0 M}{2}, \\
&\cdots
\end{aligned}
$$

and that there is no Gibbs phenomenon.

3.4 Convergence of the nonlinear subdivision scheme

We recall the following definitions.

Definition 2 Convergence of a subdivision scheme:
A dyadic subdivision scheme S is said to be uniformly convergent if

$$\forall f^0 \in l^\infty(\mathbb{Z}),\ \exists\, S^\infty f^0 \in L^\infty(\mathbb{R}) \text{ s. t. } \lim_{n\to+\infty} \sum_{j\in\mathbb{Z}} |(S^n f^0)_j - S^\infty f^0(j2^{-n})| = 0.$$

To analyze the convergence, we can use the strategy used in [3]:
A sufficient condition for the convergence of a nonlinear subdivision scheme $S_{NL} : l^\infty(\mathbb{Z}) \to l^\infty(\mathbb{Z})$ of the form:

$$\forall f^0 \in l^\infty(\mathbb{Z}), \quad \forall j \in \mathbb{Z} \qquad (S_{NL} f^0)_j = (Sf^0)_j + F(\delta f^0)_j, \tag{12}$$

where F is a nonlinear operator defined on $l^\infty(\mathbb{Z})$, δ is a linear and continuous operator on $l^\infty(\mathbb{Z})$ and S is the original linear subdivision scheme, is:

Theorem 1 *If F, S and δ given in (12) verify:*

$$\exists M > 0 \quad \textit{such that} \quad \forall f^0 \in l^\infty(\mathbb{Z}) \quad ||F(f^0)||_\infty \le M||f^0||_\infty, \tag{13}$$
$$\exists c < 1 \textit{ s. t.} \quad \forall f^0 \in l^\infty(\mathbb{Z}) \quad ||\delta S(f^0) + \delta F(\delta f^0)||_\infty \le c||\delta f^0||_\infty, \tag{14}$$

then the subdivision scheme S_{NL} is uniformly convergent.

From the definition of the scheme (11), since $||AT(x, y)||_\infty \le ||(x, y)||_\infty$ we obtain directly that $M = 1/4$. Moreover, the scheme for the differences is given by:

$$\begin{aligned}
\delta f^k_{2j-1} &= \delta f^{k-1}_j - \frac{1}{4} AT\left(\frac{\delta f^{k-1}_{j-1}}{h_{k-1}}, \frac{\delta f^{k-1}_j}{h_{k-1}}\right) h_{k-1} - \frac{1}{4} AT\left(\frac{\delta f^{k-1}_j}{h_{k-1}}, \frac{\delta f^{k-1}_{j+1}}{h_{k-1}}\right) h_{k-1},\\
\delta f^k_{2j} &= \frac{1}{2} AT\left(\frac{\delta f^{k-1}_j}{h_{k-1}}, \frac{\delta f^{k-1}_{j+1}}{h_{k-1}}\right) h_{k-1},\\
\delta f^k_{2j+1} &= \delta f^{k-1}_{j+1} - \frac{1}{4} AT\left(\frac{\delta f^{k-1}_j}{h_{k-1}}, \frac{\delta f^{k-1}_{j+1}}{h_{k-1}}\right) h_{k-1} - \frac{1}{4} AT\left(\frac{\delta f^{k-1}_{j+1}}{h_{k-1}}, \frac{\delta f^{k-1}_{j+2}}{h_{k-1}}\right) h_{k-1},\\
\delta f^k_{2j+2} &= \frac{1}{2} AT\left(\frac{\delta f^{k-1}_{j+1}}{h_{k-1}}, \frac{\delta f^{k-1}_{j+2}}{h_{k-1}}\right) h_{k-1},\\
\delta f^k_{2j+3} &= \delta f^{k-1}_{j+2} - \frac{1}{4} AT\left(\frac{\delta f^{k-1}_{j+1}}{h_{k-1}}, \frac{\delta f^{k-1}_{j+2}}{h_{k-1}}\right) h_{k-1} - \frac{1}{4} AT\left(\frac{\delta f^{k-1}_{j+2}}{h_{k-1}}, \frac{\delta f^{k-1}_{j+3}}{h_{k-1}}\right) h_{k-1}.
\end{aligned}$$

As in the previous section, lets suppose that we are working with piecewise smooth functions. We can assume that

$$\delta f_j^{k-1} = O\left(h^{k-1}\right),$$

everywhere except at the cell where the discontinuity is placed. Lets suppose now that the discontinuity affects de difference $\delta f_{j+1}^{k-1} = O\left(|f_{j+1}^{k-1} - f_j^{k-1}|\right)$. Then we can say that,

$$\left|\delta f_{2j+1}^k\right| = \left|O(|f_{j+1}^{k-1} - f_j^{k-1}|) - \frac{1}{4}AT\left(\frac{\delta f_j^{k-1}}{h_{k-1}}, \frac{\delta f_{j+1}^{k-1}}{h_{k-1}}\right)h_{k-1} - \frac{1}{4}AT\left(\frac{\delta f_{j+1}^{k-1}}{h_{k-1}}, \frac{\delta f_{j+2}^{k-1}}{h_{k-1}}\right)h_{k-1}\right| < \left(1 - O\left(h^{k-1}\right)\right)\cdot\left|\delta_{j+1}^{k-1}\right|.$$

Thus, we can conclude that the differences are contracting in the l_∞ norm,

$$||\delta f_\cdot^k||_\infty < \left(1 - O\left(h^{k-1}\right)\right)\cdot\left|\left|\delta_{j+1}^{k-1}\right|\right|_\infty.$$

3.5 Stability of the multiresolution scheme

In practice, a discrete finite sequence f^L is encoded using a multiresolution algorithm M to produce a multi-scale representation of its information contents,

$$M\left(f^L\right) = (f^0, d^1, d^2, \ldots, d^L),$$

this representation is then processed (using truncation for compression purposes) and the end result of this step is a modified multi-scale representation $(\hat{f}^0, \hat{d}^1, \hat{d}^2, \ldots, \hat{d}^L)$ which is *close* to the original one, i.e. such that (in some norm)

$$||\hat{f}^0 - f^0|| \leq \epsilon_0 \qquad ||\hat{d}^k - d^k|| \leq \epsilon_k \quad 1 \leq k \leq L,$$

where the truncation parameters $(\epsilon_0, \epsilon_1, \ldots, \epsilon_L)$ are chosen according to some criteria specified by the user.

The simplest data compression procedure is obtained by setting to zero all scale coefficients which fall below a prescribed tolerance. Let us denote

$$\hat{d}_j^k = \mathbf{tr}(d_j^k; \epsilon_k) = \begin{cases} 0 & |d_j^k| \leq \epsilon_k, \\ d_j^k & \text{otherwise}, \end{cases} \tag{15}$$

and refer to this operation as truncation (also called hard thresholding). This type of data compression is used primarily to reduce the "dimensionality" of the data.

Note that using truncation on gets,

$$|d_j^k - \hat{d_j^k}| \leq \epsilon_k.$$

After decoding the processed representation using an inverse multiresolution algorithm M^{-1}, we obtain a discrete set $\hat{f}^L$

$$\hat{f}^L = M^{-1}\left(\hat{f}^0, \hat{d}^1, \hat{d}^2, \ldots, \hat{d}^L\right)$$

$\hat{f}^L$ is expected to be *close* to the original discrete set f^L. In order for this to be true in our case, some form of stability is needed, i.e. we must require that

$$||\hat{f}^L - f^L||_1 \leq C \max(\epsilon_0, \epsilon_1, \ldots, \epsilon_L), \tag{16}$$

where C is a positive constant independent of ϵ_k and L.

On the other hand, in image applications we have boundaries. We should mention that at the boundary we propose the use of the linear scheme using information inside of the domain. In these applications we work with sequences of finite length N_k.

Some evidences of the stability:

By the definition of the scheme

$$\begin{aligned}
f_{2j-1}^k - \hat{f}_{2j-1}^k &= f_j^{k-1} - \hat{f}_j^{k-1} \\
&\quad -\frac{1}{4}\left(AT\left(\frac{\delta f_j^{k-1}}{h_{k-1}}, \frac{\delta f_{j+1}^{k-1}}{h_{k-1}}\right)h_{k-1} - AT\left(\frac{\delta \hat{f}_j^{k-1}}{h_{k-1}}, \frac{\delta \hat{f}_{j+1}^{k-1}}{h_{k-1}}\right)h_{k-1}\right) \\
&\quad +(d_j^k(f) - d_j^k(\hat{f})), \\
f_{2j}^k - \hat{f}_{2j}^k &= f_j^{k-1} - \hat{f}_j^{k-1} \\
&\quad +\frac{1}{4}\left(AT\left(\frac{\delta f_j^{k-1}}{h_{k-1}}, \frac{\delta f_{j+1}^{k-1}}{h_{k-1}}\right)h_{k-1} - AT\left(\frac{\delta \hat{f}_j^{k-1}}{h_{k-1}}, \frac{\delta \hat{f}_{j+1}^{k-1}}{h_{k-1}}\right)h_{k-1}\right) \\
&\quad -(d_j^k(f) - d_j^k(\hat{f})).
\end{aligned}$$

A standard application of the mean value theorem yields

$$AT(x, y) - AT(\bar{x}, \bar{y}) = AT_x(\tilde{x}, \tilde{y})(x - \bar{x}) + AT_y(\tilde{x}, \tilde{y})(y - \bar{y}),$$

with

$$\begin{aligned}
AT_x(x, y) &= \frac{1 + AT(x, y)^2}{2(1 + x^2)}, \\
AT_y(x, y) &= \frac{1 + AT(x, y)^2}{2(1 + y^2)},
\end{aligned}$$

for $(\tilde{x}, \tilde{y}) = (x, y) + \theta(\bar{x} - x, \bar{y} - y), \theta \in (0, 1)$. It is possible to state numerically through a graph or symbolic computation that

$$|AT(x, y)| \leq \frac{5}{2} \cdot max\{1, min\{|x|, |y|\}\}.$$

Thus, if we suppose that $|x| > |y|$, as $AT(x, y)$ is a mean, then $AT(x, y)^2 \leq |x|^2$ and

$$\frac{1 + AT(x, y)^2}{2(1 + x^2)} + \frac{1 + AT(x, y)^2}{2(1 + y^2)} \leq \frac{1}{2} + \frac{1}{2} \cdot \frac{1 + \frac{5}{2} \cdot max\{1, |y|\}}{1 + y^2}.$$

It can be easily seen that the previous expression can be bounded by,

$$\frac{1 + AT(x, y)^2}{2(1 + x^2)} + \frac{1 + AT(x, y)^2}{2(1 + y^2)} \leq \frac{11}{8}.$$

To see that this bound holds, let's suppose that $\max\{1, |y|\} = 1$, then

$$\frac{1}{2} + \frac{1}{2} \cdot \frac{1 + 2.5 \cdot max\{1, |y|\}}{1 + y^2} \leq \frac{1}{2} + \frac{1}{2} \cdot \frac{1 + \frac{5}{2}}{1 + 1} = \frac{11}{8}.$$

On the other hand, if $\max\{1, |y|\} = |y|$, then

$$\begin{aligned}
\frac{1}{2} + \frac{1}{2} \cdot \frac{1 + 2.5 \cdot max\{1, |y|\}}{1 + y^2} &= \frac{1}{2} + \frac{1}{2}\left(\frac{1}{1 + y^2} + \frac{5}{2} \cdot \frac{|y|}{1 + y^2}\right) \\
&\leq \frac{1}{2} + \frac{1}{2}\left(\frac{1}{1 + 1} + \frac{5}{2} \cdot \frac{1}{\frac{1}{|y|} + |y|}\right) \\
&\leq \frac{1}{2} + \frac{1}{2}\left(\frac{1}{2} + \frac{5}{2} \cdot \frac{1}{1 + 1}\right) = \frac{11}{8}.
\end{aligned}$$

Thus, from the properties of the trigonometric mean

$$\begin{aligned}
|f^k_{2j-1} - \hat{f}^k_{2j-1}| \leq\ & |f^{k-1}_j - \hat{f}^{k-1}_j| \\
& + \frac{11}{8}(|\delta f^{k-1}_j - \delta \hat{f}^{k-1}_j| + |\delta f^{k-1}_{j+1} - \delta \hat{f}^{k-1}_{j+1}|) \\
& + |d^k_j(f) - d^k_j(\hat{f})|, \\
|f^k_{2j} - \hat{f}^k_{2j}| \leq\ & |f^{k-1}_j - \hat{f}^{k-1}_j| \\
& + \frac{11}{8}(|\delta f^{k-1}_j - \delta \hat{f}^{k-1}_j| + |\delta f^{k-1}_{j+1} - \delta \hat{f}^{k-1}_{j+1}|) \\
& + |d^k_j(f) - d^k_j(\hat{f})|.
\end{aligned}$$

Thus

$$\begin{aligned}
||f^k - \hat{f}^k||_1 \leq\ & ||f^{k-1} - \hat{f}^{k-1}||_1 \\
& + \frac{11}{4} \sum_{j \in N_{k-1}} |\delta f^{k-1}_j - \delta \hat{f}^{k-1}_j| \\
& + ||d^{k-1}(f) - d^{k-1}(\hat{f})||_1.
\end{aligned}$$

It remains to see that the second term is well controlled in order to proof the desired stability.

Using property 2 of Lemma 1, we can say that in smooth regions, the scheme proposed is a perturbation of order $O\left((h^{k-1})^3\right)$ of the associated linear scheme. Thus, the term will be contractive plus the mentioned correction.

If f is piecewise smooth, we can find an h_0 such that the truncation parameter $\epsilon = O\left((h^k)^3\right)$ is much smaller than the jump. In this way, we assure that the details that correspond to the discontinuity will not be truncated. This is what we are going to try to assure in practice.

Figure 2 presents the compression of a piecewise smooth function contaminated with noise. At regularity zones we truncate nearly all the details. The method achieves

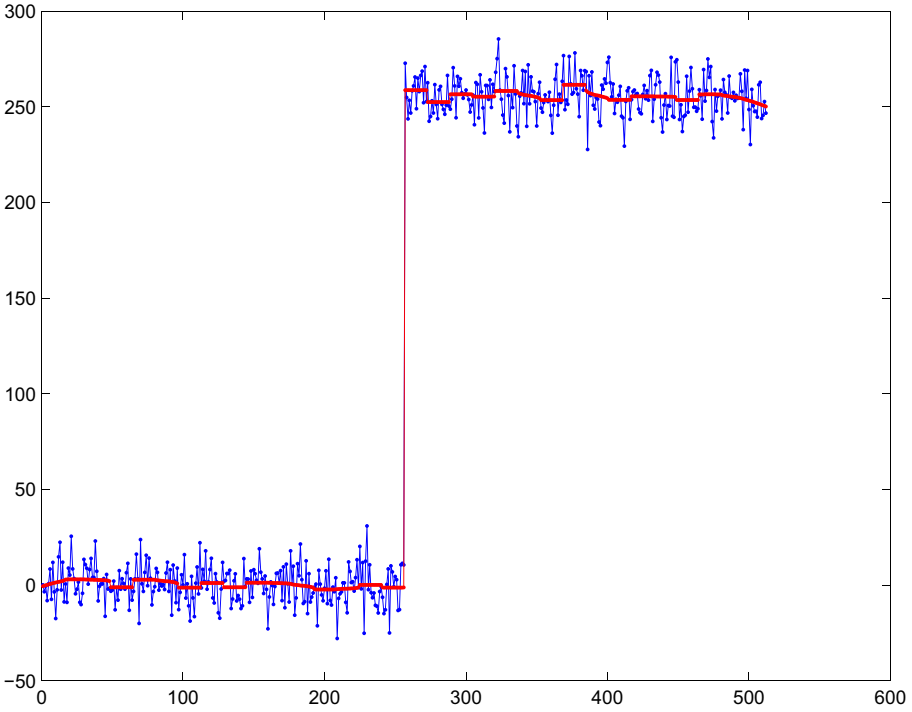

Fig. 2 The *blue signal* represents a piecewise smooth function f contaminated with noise. The *red signal* represents the reconstructed signal $\hat{f}$

a performance similar to the one obtained by the linear algorithm. The truncation parameter is chosen such that at the discontinuity we keep the important details. Due to the nonlinear character of the trigonometric mean, near the discontinuity we attain adaption.

Estimation of the stability constant:

Finally, we estimate numerically the stability constant for both linear and nonlinear schemes. In order to estimate numerically the stability constant for the l_1-norm, we consider the following setup: Given a discrete sequence $f^L = (f_j^L)$, we descend in the multiresolution pyramid obtaining its multiresolution representation $Mf^L = \{f^0, d^1, \ldots, d^L\}$ ($L = 4$ in our numerical test). We truncate the detail coefficients of this representation which are larger than a certain tolerance parameter ϵ obtaining the perturbed representation $\{\hat{f}^0, \hat{d}^1, \ldots, \hat{d}^L\}$. We then measure the size of the perturbation by

$$\mu = ||f^0 - \hat{f}^0||_1 + \sum_{k=1}^{L} ||d^k - \hat{d}^k||_1. \tag{17}$$

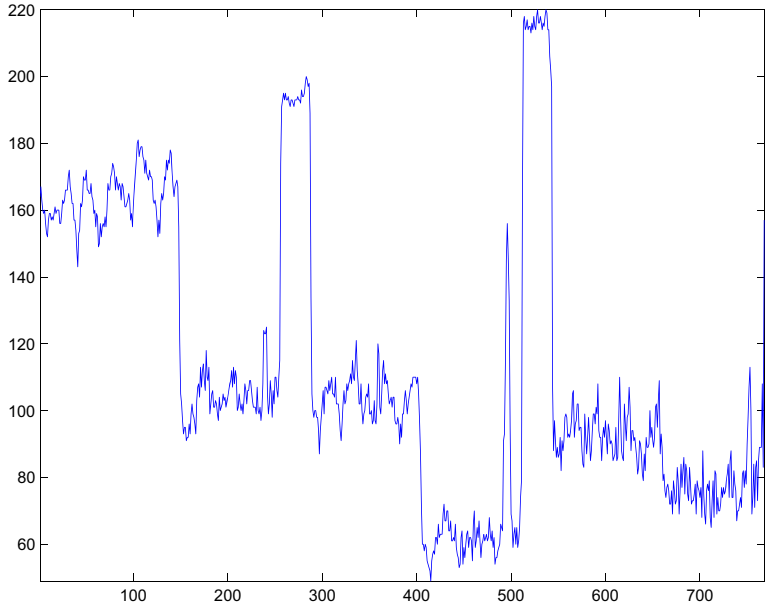

Fig. 3 Row 256 of the *Red House* image

Next, we use the decoding algorithm to obtain an approximation given by $\hat{f}^L = M^{-1}\{\hat{f}^0, \hat{d}^1, \ldots, \hat{d}^L\}$ to the original discrete sequence. We measure the error committed as

$$E_a = ||f^L - \hat{f}^L||_1. \tag{18}$$

A numerical estimation of the stability constant is provided by the ratio $C_s = \frac{E_a}{\mu}$. We have considered the sequence given by a row of the *Red House* image in Fig. 3. In Table 2 we display the results of our numerical test, comparing the results obtained by the new algorithm to those obtained by the linear analogue algorithm. The estimations obtained for different levels of compression are similar for both cases. The linear algorithm corresponds to biorthogonal wavelets, so the similarity between the results could be intuitively explained through the stability of the nonlinear algorithm.

Table 2 Estimations of the stability constant for different values of the truncation parameter ϵ, with $L = 4$ multiresolution levels

ϵ	0.1	0.5	1	10	20	50
AT	1.0992	0.9150	0.7880	0.5596	0.5827	0.5661
Linear	1.0630	0.9118	0.7781	0.5819	0.5908	0.5835

Row 256 of the *Red House* image

4 Experiments with colour images using cell-average multiresolution schemes

In this section we will compare the results obtained using the proposed new nonlinear method versus those obtained by PPH and the corresponding linear scheme.We will present the results of the comparison between a linear compression method and the new algorithm proposed. We will also present a brief comparison of the new method with the PPH method.

We will use the *PSNR* as a numerical estimator to measure the quality of the resulting compressed images. We consider the RGB colour model, we present the numerical results obtained for each colour band and also for the global image. In general, the results for each band present some differences because of the different colour properties of each band.

We apply the one-dimensional transform to images via the classical two dimensional tensor product approach [20] to generate the 2D multiresolution algorithm. Let Mf^L be the tensor-product multiresolution representation of the two dimensional array $f^L = (f^L_{i,j})^{J_L}_{(i,j)=1}$.

As mentioned before, applying the inverse multiresolution transform M^{-1} to the truncated version of the direct multiresolution of f^L denoted by $\mathbf{tr}^\epsilon(Mf^L)$, where ϵ represents the truncation parameter, we compute $\hat{f}^L = M^{-1}\mathbf{tr}^\epsilon(Mf^L)$.

We then compute the *PSNR* (Peak Signal Noise Ratio), which is a measure widely used for the estimation of the quality of the reconstructed image [23]. For an 8 bit image $(0-255)$,

$$PSNR = 20\log_{10}\left(\frac{255}{||f^L - \hat{f}^L||_{l_2}}\right).$$

A higher *PSNR* number implies a better quality.

It is important to remark how the scheme behaves at the boundaries. Several options are possible, but we have chosen to apply non centered Lagrange operators. More specifically, the prediction operators for the left and right boundary are,

$$\begin{aligned} f^k_1 &= \frac{11}{8}f^{k-1}_1 - \frac{4}{8}f^{k-1}_2 + \frac{1}{8}f^{k-1}_3 \\ f^k_{2n-1} &= \frac{1}{8}f^{k-1}_{n-2} + \frac{4}{8}f^{k-1}_{n-1} + \frac{5}{8}f^{k-1}_n, \end{aligned}$$

being n the index of the last element of the scale $k-1$.

4.1 Eliminating Gibbs oscillations and numerical artifacts

The images *Red House* and *Drawing1*, presented in Fig. 4, have been selected to perform the experiments. They will allow us to compare between the linear and nonlinear schemes.

Lets start our test with the *Red House* image. Table 3 shows the results obtained for a truncation parameter $\epsilon = 25$ (as explained previously, we have used the *hard thresholding* shown in (15) to reduce the dimensionality of the data). In this table we can see for each colour band of the image the number of coefficients that we

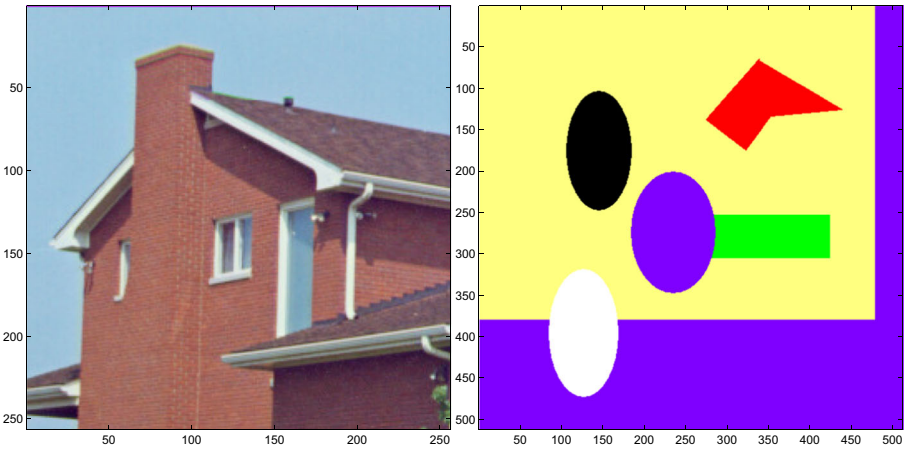

Fig. 4 *Left Red House* image. *Right Drawing 1* image

have kept (keep in mind that keeping 1000 coefficients for an image of 256×256 pixels means keeping around the 1.5% of the original information), the l_1 norm and PSNR. The results presented for both methods are similar. This conclusion can also be reached if we look at Table 4, where the previous information is presented for the global image (not separated for each colour band).

Even though, it is fair to compare the results using the same number of coefficients for each colour band. Thus, if we set the number of coefficients kept for each band to those obtained by the new method using a truncation parameter of $\epsilon = 25$, we obtain the results shown in Table 5. As before, we present the information corresponding to the whole image in Table 6. It can be seen that the results are quite similar in compression, l_1 norm and PSNR. Even though, the quality of an image is not only evaluated making use of estimators as the PSNR. It is also very important to evaluate the presence of numerical effects such as Gibbs phenomenon or diffusion

Table 3 *Red House* Image : Number of significant coefficients, l_1 norm of the compression error, *PSNR* quality estimator, number of multiresolution levels $L = 4$, truncation parameter $\epsilon = 25$

$\epsilon = 25$			
New method	RED	GREEN	BLUE
nnz	879	1436	1202
l_1	5.2899	5.1896	5.1427
PSNR	30.2815	29.8392	29.9011
Linear	RED	GREEN	BLUE
nnz	862	1495	1251
l_1	5.4377	5.7336	5.5812
PSNR	30.3948	29.7342	29.6499

Table 4 *Red House* Image: Number of significant coefficients, l_1 norm of the compression error, *PSNR* quality estimator, number of multiresolution levels $L = 4$, truncation parameter $\epsilon = 25$

$\epsilon = 25$		
	New method	Linear
nnz	3517	3608
l_1	5.2900	5.5841
PSNR	30.0029	29.9138

of discontinuities. Using the previous configuration (i.e. setting the number of coefficients kept for each band to those obtained by the new method using a truncation parameter of $\epsilon = 25$), we obtain the approximations shown in Fig. 5 for the linear and the new scheme (Table 5 shows the number of coefficients used for each band: 879, 1436 and 1202 for the red, green and blue bands respectively). In Fig. 6 we present a zoom of the results, where the differences are evident. In the approximation obtained by the linear scheme, we can observe several numerical effects that are not present in the result obtained by the new method. The numerical effects that appear in the result obtained by the linear method are a consequence of using the same kind of reconstruction in the whole image, without making a special treatment at the edges between objects. The new method tries to adapt to discontinuities in order to avoid edge diffusion and Gibbs effect, that always appear in linear reconstructions.

Lets try to analyze now the result of the new algorithm applied to geometrical images. Now our tests will be focussed on the image *Drawing 1* shown in Fig. 4 (right). This image is a geometric image synthetically obtained. In this case, we are not dealing with diffused edges anymore. All the discontinuities in this image are clearly defined in the original image. As before, for the first experiment we set the truncation parameter to $\epsilon = 25$. The numerical results obtained for both compression

Table 5 *Red House* Image: Number of significant coefficients, l_1 norm of the compression error, *PSNR* quality estimator, number of multiresolution levels $L = 4$

$\epsilon = 25$			
New method	RED	GREEN	BLUE
nnz	879	1436	1202
l_1	5.2899	5.1896	5.1427
PSNR	30.2815	29.8392	29.9011
Linear	RED	GREEN	BLUE
nnz	879	1436	1202
l_1	5.4074	5.8277	5.6559
PSNR	30.4530	29.5610	29.5148

Table obtained fixing the number of significant coefficients to those resulting from compressing the image with the new algorithm setting the truncation parameter to $\epsilon = 25$

Table 6 *Red House* Image: Number of significant coefficients, l_1 norm of the compression error, *PSNR* quality estimator, number of multiresolution levels $L = 4$

$\epsilon = 25$		
	New method	Linear
nnz	3517	3517
l_1	5.2900	5.4074
PSNR	30.0029	29.8220

Table obtained fixing the number of significant coefficients to those resulting from compressing the image with the new algorithm setting the truncation parameter to $\epsilon = 25$

methods analysed are presented in Table 7. As it could be expected, in this Table we can find that the results obtained by the new method clearly outperform the linear method. This is in accordance with the reconstructed images shown in Fig. 7.

As before, in order to compare more efficiently the performance of the two algorithms, we show Table 8. In this table we present the *PSNR*, the mean of the error and the total number of significant coefficients obtained by both methods for the global image. The conclusions are the same: the results obtained by the new method are clearly better than those obtained by the linear method. As previously, now we can set the coefficients kept to those obtained by the new method. These coefficients are shown in Table 9 (1579, 2758 and 1602 respectively for the red, green and blue bands). In this case the conclusions that we can reach are even clearer than before: the new method outperform the results obtained by the linear method for geometrical images. As it is shown in Table 3, the same conclusions can be obtained when fixing the number of coefficients for both methods.

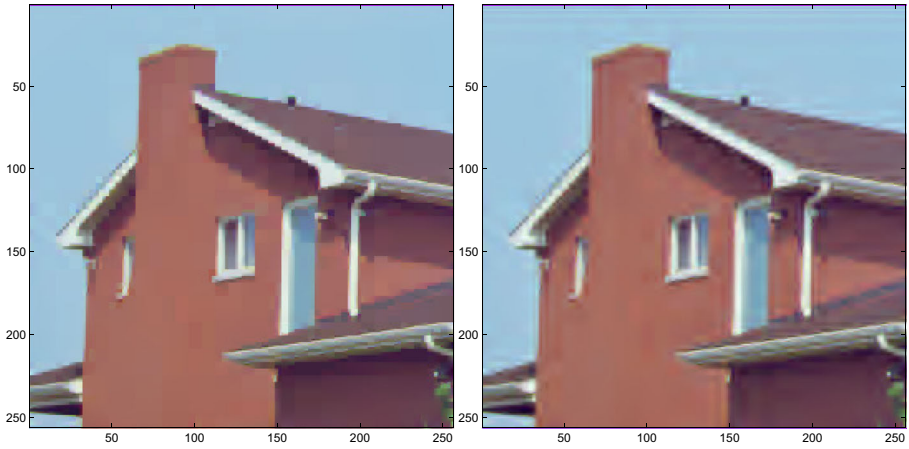

Fig. 5 *Left*, reconstruction of *Red House* image using the new algorithm. *Right*, reconstruction using linear method. Number of multiresolution levels, $L = 4$. Number of coefficients set equal to those obtained by the new algorithm for $\epsilon = 25$ and shown in Table 5

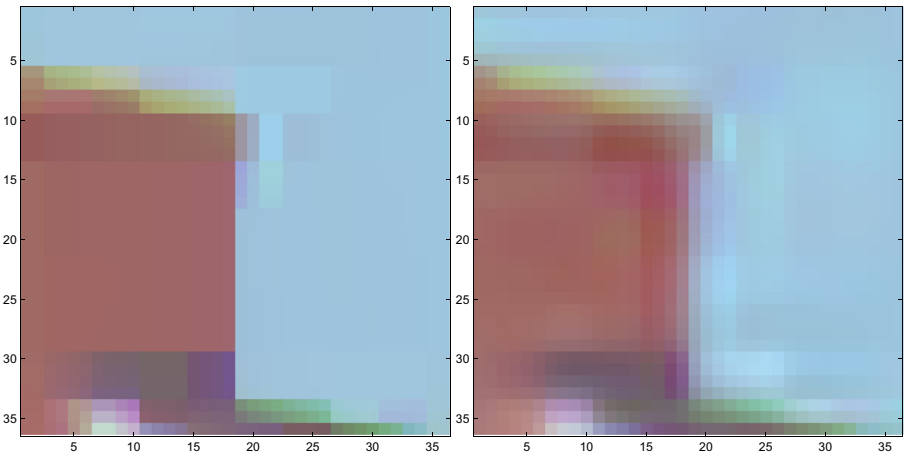

Fig. 6 *Left*, zoom obtained from the reconstruction of *Red House* image using the new algorithm. *Right*, zoom from the reconstruction using linear method. Number of multiresolution levels, $L = 4$. Number of coefficients set equal to those obtained by the new algorithm for $\epsilon = 25$ and shown in Table 5

As mentioned before, in order to estimate the visual quality of an image, it is not enough to obtain quality indicators such as the PSNR. It is also very important that the resulting compressed images are free of unwanted numerical effects. If we look at the reconstructed images (Figs. 7, 8, 9), we observe that at the edges of the results obtained by the linear method we can find several zones affected by Gibbs effect and diffusion that do not appear in the reconstructions obtained by the new method. This is due to the fact that the *Trigonometric Mean* eliminates Gibbs effect and reduces edge diffusion that are impossible to avoid if we are working with linear reconstructions. It is also very important to mention that the stair case shown in Fig. 8 is perfectly reconstructed by the nonlinear method.

Table 7 *Drawing 1* Image: Number of significant coefficients, l_1 norm of the compression error, *PSNR* quality estimator, number of multiresolution levels $L = 4$

$\epsilon = 25$			
New method	RED	GREEN	BLUE
nnz	1579	2758	1602
l_1	0.20897	0.14584	0.36059
PSNR	40.3284	44.3036	37.3427
Linear	RED	GREEN	BLUE
nnz	2951	5005	2637
l_1	0.78165	0.54495	1.1661
PSNR	38.1659	38.6556	36.2499

Table obtained for $\epsilon = 25$

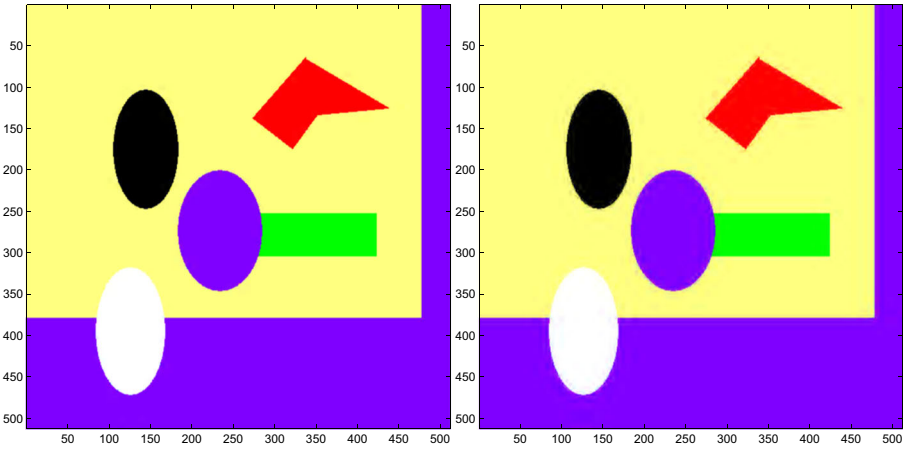

Fig. 7 *Left*, reconstruction of *Drawing 1* image using the new algorithm. *Right*, reconstruction using linear method. Number of multiresolution levels, $L = 4$. Number of coefficients set equal to those obtained by the new algorithm for $\epsilon = 25$ and shown in Table 9

Table 8 *Drawing 1* Image: Number of significant coefficients, l_1 norm of the compression error, *PSNR* quality estimator, number of multiresolution levels $L = 4$

$\epsilon = 25$		
	New method	Linear
nnz	5939	10593
l_1	0.2385	0.8309
PSNR	39.7988	37.5616

Table obtained for $\epsilon = 25$

Table 9 *Drawing 1* Image: Number of significant coefficients, l_1 norm of the compression error, *PSNR* quality estimator, number of multiresolution levels $L = 4$

$\epsilon = 25$			
New method	RED	GREEN	BLUE
nnz	1579	2758	1602
l_1	0.20897	0.14584	0.36059
PSNR	40.3284	44.3036	37.3427
Linear	RED	GREEN	BLUE
nnz	1579	2758	1602
l_1	1.4802	1.232	1.7635
PSNR	32.9199	32.6345	33.2368

Table obtained fixing the number of significant coefficients to those resulting from compressing the image with the new algorithm setting the truncation parameter to $\epsilon = 25$

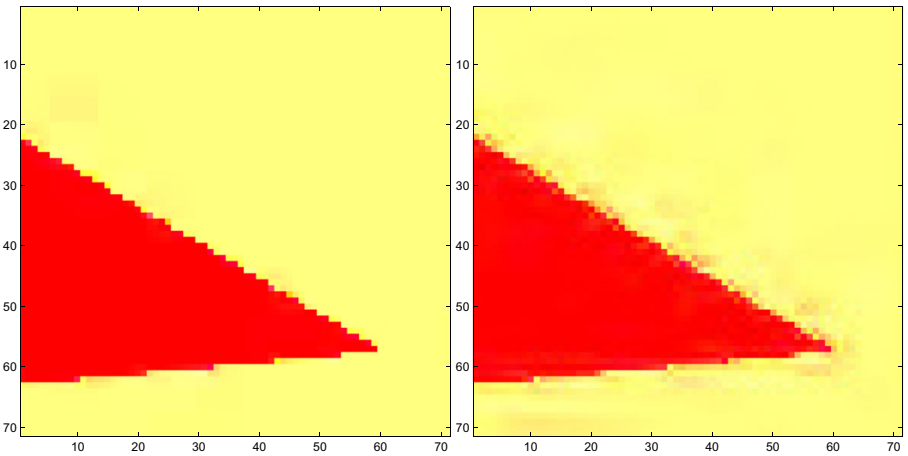

Fig. 8 *Left*, zoom obtained from the reconstruction of *Drawing 1* image using the new algorithm. *Right*, zoom from the reconstruction using linear method. Number of multiresolution levels, $L = 4$. Number of coefficients set equal to those obtained by the new algorithm for $\epsilon = 25$ and shown in Table 9

Now we will show a comparison of the new method versus the PPH method. In particular we will present some numerical results obtained applying the new method and the PPH method to the images presented in Fig. 4.

Lets start our test with the *Red House* image. As in previous section, it is fair to compare the results using the same number of coefficients for each colour band. Thus, if we set again the number of coefficients kept for each band to those obtained by the new method using a truncation parameter of $\epsilon = 25$, we obtain results for the whole image that are quite similar in compression, l_1 norm and PSNR (as an example, we can say that for this image we obtain as PSNR 30.0029 for the new scheme and

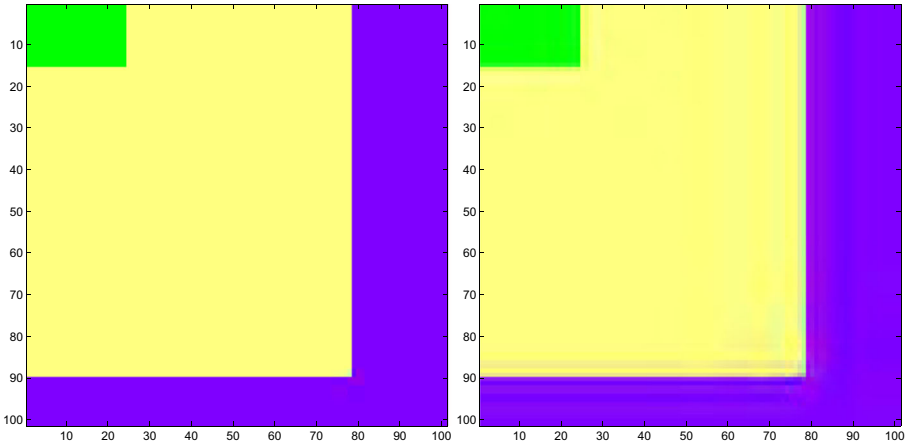

Fig. 9 *Top left*, zoom obtained from the reconstruction of *Drawing 1* image using the new algorithm. *Top right*, zoom from the reconstruction using linear method. Number of multiresolution levels, $L = 4$. Number of coefficients set equal to those obtained by the new algorithm for $\epsilon = 25$ and shown in Table 9

Table 10 *Drawing 1* Image: Number of significant coefficients, l_1 norm of the compression error, *PSNR* quality estimator, number of multiresolution levels $L = 4$

$\epsilon = 25$		
	New method	Linear
nnz	5939	5939
l_1	0.2385	1.4919
PSNR	39.7988	32.9235

Table obtained fixing the number of significant coefficients to those resulting from compressing the image with the new algorithm setting the truncation parameter to $\epsilon = 25$

30.0025 for the PPH). The tests that we have performed resulted in no appreciable difference for the visual image quality. Thus, for shortness, in this experiment we will not present image examples or tables.

Now our tests will be focussed on the image *Drawing 1* shown in Fig. 4 to the right. The results obtained show again that the PPH and the new method obtain similar results, but they outperform the results obtained by the linear method for geometrical images. As an example, we can say that the PSNR obtained for the new scheme was 39.7988 and for the PPH 39.7986. As before, for shortness, in this experiment we will not present image examples or tables.

5 Conclusions

From all these results we can take out the following conclusions:

On the one hand, having a multiresolution matrix composed by the same number of significant coefficients, the new nonlinear method proposed obtains similar quality as the linear method in *PSNR* if we work with real images. On the other hand, as it has been shown in the experiments, the result of the linear method shows unwanted numerical effects that are not observed when using the new method. For geometrical images, the nonlinear method clearly outperforms the results obtained by the linear method. The new method proposed avoids the order reduction inherent to PPH interpolation but keeping the capacity of eliminating Gibbs phenomenon and diffusion.

Acknowledgments We would like to thank the referees for their useful comments and their help to improve this paper.

Conflict of interest The authors declare that they have no conflict of interest.

References

1. Amat, S., Cherif, H., Trillo, J.C.: Denoising using Linear and nonlinear multiresolutions. Eng. Comput. **22**(7), 877–891 (2005)

2. Amat, S., Ruiz, J., Trillo, J.C.: Denoising using linear and nonlinear multiresolutions II: Cell-average framework and color images. Eng. Comput. **26**(7), 806–827 (2009)
3. Amat, S., Dadourian, K., Liandrat, J.: Analysis of a class of nonlinear subdivision schemes and associated multiresolution transforms. Adv. Comput. Math. **34**(3), 253–277 (2011)
4. Amat, S., Dadourian, K., Liandrat, J.: On a nonlinear subdivision scheme avoiding Gibbs oscillations and converging towards Cs functions with $s > 1$. Math. Comp. **80**(274), 959–971 (2011)
5. Amat, S., Dadourian, K., Liandrat, J.: Analysis of a class of nonlinear subdivision schemes and associated multiresolution transforms. Adv. Comput. Math. **34**(3), 253–277 (2011)
6. Amat, S., Donat, R., Liandrat, J., Trillo, J.C.: Analysis of a new nonlinear subdivision scheme. Applications in image processing. Found. Comput. Math. **6**(2), 193–225 (2006)
7. Amat, S., Donat, R., Liandrat, J., Trillo, J.C.: A fully adaptive multiresolution scheme for image processing. Math. Comput. Modell **46**(1–2), 2–11 (2007)
8. Amat, S., Liandrat, J.: On the stability of the PPH nonlinear multiresolution. Appl. Comp. Harm. Anal. **18**(2), 198–206 (2005)
9. Amat, S., Liandrat, J., Ruiz, J., Trillo, J.C. S$\vec{e}$MA J. **60**, 75–92 (2012)
10. Aràndiga, F., Donat, R.: Nonlinear multi-scale decomposition: The approach of A.Harten. Numer. Algorithms **23**, 175–216 (2000)
11. Binev, P., Dahmen, W., DeVore, R., Dyn, N.: Adaptive approximation of curves. Approximation theory: a volume dedicated to Borislav Bojanov, pp. 43–57. Prof. M. Drinov Acad Publ. House, Sofia (2004)
12. Chambolle, A., DeVore, R.A., Lee, N., Lucier, B.J.: Nonlinear wavelet image processing: variational problem, compression and noise removal through wavelet shrinkage. IEEE Trans. Image Process. **7**, 319–335 (1998)
13. Cohen, A.: Theoretical, Applied and Computational Aspects of Nonlinear approximation. (English Summary) Multiscale Problems and Methods in Numerical Simulations, vol. 1–29, Lecture Notes in Math, pp. 1825. Springer, Berlin (2003)
14. Cohen, A., DeVore, R., Petrushev, P., Xu, H.: Nonlinear approximation and the space $\mathrm{BV}(R^2)$. Amer. J. Math. **121**(3), 587–628 (1999)
15. Cohen, A., Dyn, N., Matei, B.: Quasi linear subdivision schemes with applications to ENO interpolation. Appl. Comput. Harmonic Anal. **15**, 89–116 (2003)
16. Daubechies, I., Runborg, O., Sweldens, W.: Normal multiresolution approximation of curves. Const. Approx. **20**(3), 399–463 (2004)
17. Donoho, D.L., Johnstone, I.: Ideal spatial adaptation by wavelet shrinkage. Biometrika **81**, 425–455 (1994)
18. Gottlieb, D., Shu, C.-W.: On the Gibbs phenomenon and its resolution. SIAM Rev. **39**(4), 644–668 (1997)
19. Harten, A.: Multi resolution representation of data II. SIAM J. Numer. Anal. **33**(3), 1205–1256 (1996)
20. Harten, A., Yad-Shalom, I.: Fast multiresolution algorithms for matrix-vector multiplications. SIAM J. Numer. Anal. **31**, 1191–1218 (1994)
21. Matei, B.: Smoothness characterization and stability in nonlinear multiscale framework: theoretical results. Asymptot. Anal. **41**(3–4), 277–309 (2005)
22. Oswald, P.: Smoothness of nonlinear median-interpolation subdivision. Adv. Comput. Math. **20**(4), 401–423 (2004)
23. Rabbani, M., Jones, P.W.: Digital Image Compression Techniques. Tutorial Text, Society of Photo-Optical Instrumentation Engineers (SPIE), TT07 (1991)